η transition form factor: a combined analysis of space- and time-like experimental data through rational approximants

Rafel Escribano[1,2;1)]

[1] Grup de Física Teòrica, Departament de Física, Universitat Autònoma de Barcelona, E-08193 Bellaterra (Barcelona), Spain
[2] Institut de Física d'Altes Energies (IFAE), The Barcelona Institute of Science and Technology, Campus UAB, E-08193 Bellaterra (Barcelona), Spain

Abstract: A combined analysis of the space- and time-like experimental data for the η transition form factor is performed in a model-independent way by means of rational approximants. The recent measurement of the e^+e^- invariant mass spectrum of the $\eta \to e^+e^-\gamma$ decay provided by the A2 Collaboration allowed us to extract the most precise and up-to-date slope and curvature parameters of the form factor. The impact of this new analysis on the η-η' mixing parameters and the $VP\gamma$ couplings is also discussed.

Key words: η transition form factor, space- and time-like data analysis, rational approximants, slope and curvature parameters, η-η' mixing, $V \to P\gamma$ radiative decays

PACS: 13.40.Gp, 13.20.Jf, 12.40.Vv

1 Introduction

The pseudoscalar transition form factors (TFFs) describe the effect of the strong interaction on the $\gamma^*\gamma^*P$ vertex, where $P = \pi^0, \eta, \eta', \eta_c \ldots$, and is represented by $F_{P\gamma^*\gamma^*}(q_1^2, q_2^2)$, a function of the photon virtualities q_1^2, and q_2^2. From the experimental point of view, one can study such TFFs from both space- and time-like energy regions. The time-like region of the TFF can be accessed at meson facilities either through the double Dalitz decay processes $P \to l^+l^-l^+l^-$, which give access to both photon virtualities (q_1^2, q_2^2) in the range $4m_l^2 < (q_1^2, q_2^2) < (m_P - 2m_l)^2$, or the single Dalitz decay processes $P \to l^+l^-\gamma$, which contains a single virtual photon with transferred momentum in the range $4m_l^2 < q_1^2 < m_P^2$, thus simplifying the TFF to $F_{P\gamma^*\gamma^*}(q_1^2, 0) \equiv F_{P\gamma^*\gamma}(q^2)$. To complete the time-like region, e^+e^- colliders access to the values $q^2 > m_P^2$ through the $e^+e^- \to P\gamma$ annihilation processes. The space-like region of the TFFs are accessed in e^+e^- colliders by the two-photon-fusion reaction $e^+e^- \to e^+e^-P$, where at the moment the measurement of both virtualities is still an experimental challenge. The common practice is then to extract the TFF when one of the outgoing leptons is tagged and the other is not, that is, the single-tag method. The tagged lepton emits a highly off-shell photon with transferred momentum $q_1^2 \equiv -Q^2$ and is detected, while the other, untagged, is scattered at a small angle with $q_2^2 \simeq 0$. The form factor extracted from the single-tag experiment is then $F_{P\gamma^*\gamma^*}(-Q^2, 0) \equiv F_{P\gamma^*\gamma}(Q^2)$.

At low-momentum transfer, the TFF can be described by the expansion

$$F_{P\gamma^*\gamma}(Q^2) = F_{P\gamma\gamma}(0)\left(1 - b_P\frac{Q^2}{m_P^2} + c_P\frac{Q^4}{m_P^4} + \cdots\right) , \quad (1)$$

where $F_{P\gamma\gamma}(0)$ is the normalization, the low-energy parameters (LEPs) b_P and c_P are the slope and the curvature of the TFF, respectively, and m_P is the pseudoscalar meson mass. $F_{P\gamma\gamma}(0)$ can be obtained either from the measured two-photon partial width of the meson P or, in the case of π^0, η and η', from the prediction of the axial anomaly in the chiral limit of QCD.

The slope parameter has been extensively discussed from both theoretical analyses [1–5] and experimental measurements [6–12]. With respect to the experimental determinations, the values for the slope are usually obtained after a fit to data using a normalized, single-pole term with an associated mass Λ_P, *i.e.*

$$F_{P\gamma^*\gamma}(Q^2) = \frac{F_{P\gamma\gamma}(0)}{1 + Q^2/\Lambda_P^2} . \quad (2)$$

The A2 Collaboration reported $b_\eta = 0.59(5)$ [12], the most precise experimental determination up to date. The curvature was for the first time reported in Ref. [3] with the value $c_\eta = 0.37(10)_{\rm stat}(7)_{\rm sys}$.

Several attempts to describe the η TFF are available in the literature at present [2, 4, 5, 13–27] but none of them tries for a unique description of both space- and time-like experimental data, specially at low energies. In Ref. [28], it was suggested for the π^0 case that a model-independent approach to the space-like TFF can be achieved using a sequence of rational functions, the

Received 30 Nov. 2015

1) E-mail: rescriba@ifae.es

Padé Approximants (PAs), to fit the data. Later on, in Ref. [3], the same method was applied to the η and η' TFFs. More recently, the A2 Collaboration reported a new measurement of the $\eta \to e^+e^-\gamma$ Dalitz decay process with the best statistical accuracy up to date [12]. A comparison with different theoretical approaches was also performed. In particular, the results from Ref. [3], based on space-like data, were extrapolated to the time-like region and agreed perfectly with their measurement. Triggered by these new A2 results, we explore in the present work a combined description of both space- and time-like regions of the η TFF within our method of rational approximants. This will provide, for the first time, a determination of the energy dependence of the η TFF in both regions together with a unified extraction of its LEPs.

Our approach makes use of PAs as fitting functions to all the experimental data. PAs are rational functions $P^N_M(Q^2)$ (ratio of a polynomial $T_N(Q^2)$ of order N and a polynomial $R_M(Q^2)$ of order M) constructed in such a way that they have the same Taylor expansion as the function to be approximated up to order $\mathcal{O}(Q^2)^{N+M+1}$ [29]. Since PAs are built in our case from the unknown low-energy parameters (LEPs) of the TFF, once the fit to the experimental data is done, the reexpansion of the PAs yields the desired coefficients. The advantage of PAs over Taylor expansions is their ability to enlarge the domain of convergence. However, to prove the convergence of a given PA sequence is a difficult task and only for certain classes of functions this can be done rigorously. In practice, the success of PAs in the description of experimental data can only be seen *a posteriori* in the sense that the pattern of convergence can be shown but unfortunately not proven mathematically. We refer the interested reader to Refs. [30, 31] for details on this technique.

2 η transition form factor: a space- and time-like description

To extract the η TFF low-energy parameters b_η and c_η (slope and curvature, respectively) from the available data, we start with a $P^L_1(Q^2)$ sequence. However, according to Ref. [32], the pseudoscalar TFFs behave as $1/Q^2$ for $Q^2 \to \infty$, which means that, for any value of L, one will obtain in principle a good fit only up to a finite value of Q^2 but not for $Q^2 \to \infty$. Therefore, it would be desirable to incorporate this asymptotic-limit information in the fits to $Q^2F_{\eta\gamma^*\gamma}(Q^2)$ by considering also a $P^N_N(Q^2)$ sequence.

Experimental data from the space-like region is obtained from CELLO, CLEO, and BABAR Collaborations [7, 8, 33], together with the time-like experimental data from NA60 and A2 Collaborations [9, 10, 12]. We also include the value $\Gamma_{\eta\to\gamma\gamma} = 0.516(18)$ keV [34] (which is basically dominated by the recent KLOE-2 measurement [35]) in our fits.

We start fitting with a $P^L_1(Q^2)$ sequence. We reach $L = 7$ and we show it in Fig. 1 as a green-dashed line. The smaller plot in Fig. 1 is a zoom into the time-like region. The obtained LEPs are shown in Fig. 2 together with our previous results (empty orange) when only space-like data were included in our fits [3]. The stability observed for the LEPs with the $P^L_1(Q^2)$ sequence is remarkable, and the impact of the inclusion of time-like data is clear since not only allows us to reach higher precision on each PA but also to enlarge our PA sequence by 2 elements. The stability of the result is also clearer and reached earlier, reduces our systematic error, and shows the ability of our method to extract, for the first time, the LEPs from a combined fit to all the available data.

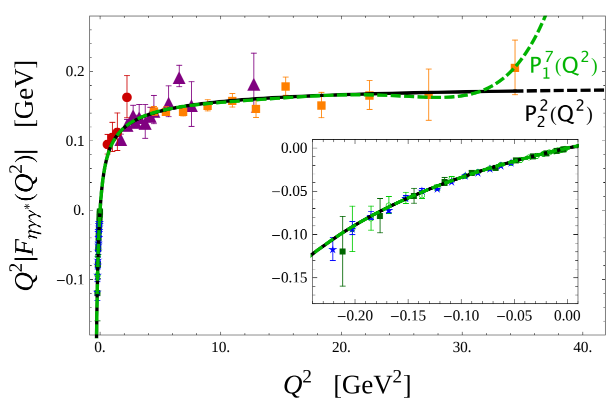

Fig. 1. η-TFF best fits. Green-dashed line shows our best $P^L_1(Q^2)$ fit and black line our best $P^N_N(Q^2)$ fit. Experimental data points in the space-like region are from CELLO (red circles) [7], CLEO (purple triangles) [8], and BABAR (orange squares) [33] Collaborations. Experimental data points in the time-like region are from NA60 (blue stars) [9], A2 2011 (dark-green squares) [10], and A2 2013 (empty-green circles) [12]. The inner plot shows a zoom into the time-like region.

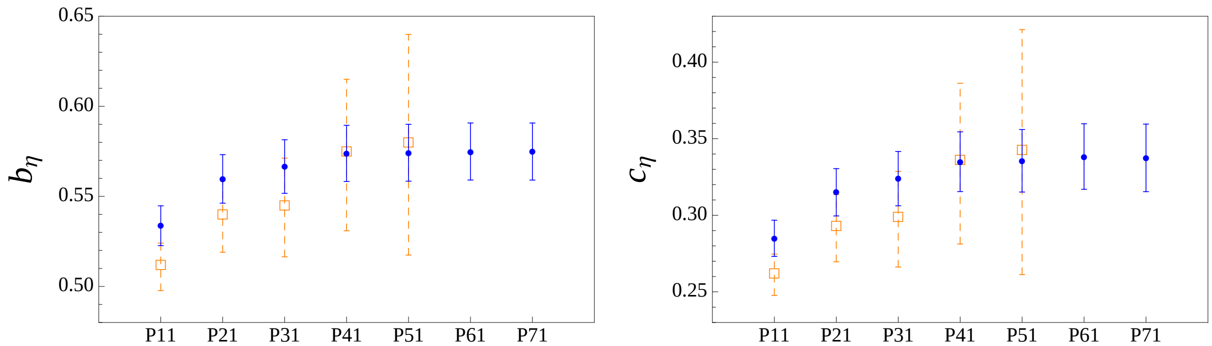

Fig. 2. Slope (left panel) and curvature (right panel) predictions for the η TFF using the $P_1^L(Q^2)$ up to $L=7$ (blue points). Previous results considering only space-like data from Ref. [3] are also shown (empty-orange squares) as a way to stress the role of the time-like data in our fits. Only statistical errors are shown..

To reproduce the asymptotic behavior of the TFF, we have also considered the $P_N^N(Q^2)$ sequence. The results obtained are in very nice agreement with our previous determinations. The best fit is shown as black-solid line in Fig. 1. We reach $N=2$. Since these approximants contain the correct high-energy behavior built-in, they can be extrapolated up to infinity (black-dashed line in Fig. 1) and then predict the leading $1/Q^2$ coefficient:

$$\lim_{Q^2\to\infty} Q^2 F_{\eta\gamma^*\gamma}(Q^2) = 0.177^{+0.020}_{-0.009}\ \text{GeV}\ . \tag{3}$$

This prediction, although larger than in our previous work [3], still cannot be satisfactorily compared with the BABAR time-like measurement at $q^2 = 112$ GeV^2, $F_{\eta\gamma^*\gamma}(112\ \text{GeV}^2) = 0.229(30)(8)$ GeV [36]. The impact of such discrepancy in the $\eta-\eta'$ mixing is discussed in the next section.

Our combined weighted average results, taking into account both types of PA sequences, give

$$\begin{cases} b_\eta = 0.576(11)_{\text{stat}}(4)_{\text{sys}} \\ c_\eta = 0.339(15)_{\text{stat}}(5)_{\text{sys}} \end{cases} \tag{4}$$

where the second error is systematic (around 0.7 and 1.5% for b_P and c_P, respectively.

Equation (4) can be compared with $b_\eta = 0.60(6)_{\text{stat}}(3)_{\text{sys}}$ and $c_\eta = 0.37(10)_{\text{stat}}(7)_{\text{sys}}$ using space-like data exclusively [3]. As expected, not only statistical results have been improved but also systematics, both by an order of magnitude, yielding the most precise slope determination ever.

Our slope is compared with experimental determinations from [6–12] together with theoretical extraction from [1–5, 37, 38] in Fig. 3.

One should notice that all the previous collaborations used a VMD model fit to extract the slope. In order to be consistent when comparing with our results, a systematic error of about 40% should be added to the experimental determinations based on space-like data [3, 28], and a systematic error of about 5% should be added to the experimental determinations based on time-like data..

When comparing different theoretical extractions of the slope of the η TFF with our result in Fig. 3, we find a pretty good agreement with the exception of the results in Ref. [2] that reported $b_\eta = 0.546(9)$ and $b_\eta = 0.521(2)$ using Resonance Chiral Theory with one- or two-octet ansätze. The disagreement is between 2 and 5 standard deviations. Reference [2] uses Resonance Chiral Theory, which is based in large-N_c arguments, to extract LEPs. Going from large-N_c to $N_c = 3$ imposes a systematic error [31, 39–41]. Since Ref. [2] considered two approximations for fitting the η TFF (with one and two octets), one could consider the difference between them as a way to estimate such error [3, 42]. In such a way, the η TFF slope would read $b_\eta = 0.53(1)$, at 2.5 standard deviation from our result.

Eventually, we want to comment on the effective single-pole mass determination Λ_P from Eq. (2). Using $b_P = m_P^2/\Lambda_P^2$ and the values in Eq. (4), we obtain $\Lambda_\eta = 0.722(7)$ GeV or $\Lambda_\eta^{-2} = 1.919(39)$ GeV^{-2}.

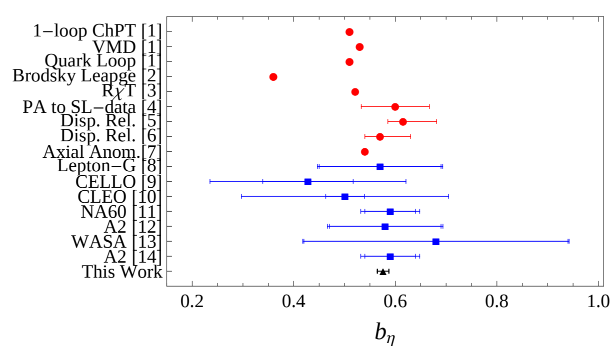

Fig. 3. Slope determinations for η TFF from different theoretical (red circles) and experimental (blue squares) references discussed in the text. Inner error is the statistical one and larger error is the combination of statistical and systematic errors.

The fits shown in Fig. 1 use the experimental value of the two-photon decay width as an experimental datum to be fitted. Such fit could be repeated without including that decay. In such a way, we reach again a $P_1^7(Q^2)$ and a $P_2^2(Q^2)$ as our best PA with the advantage now that the value $F_{\eta\gamma\gamma}(0)$ is a prediction of our fits. We find $F_{\eta\gamma\gamma}(0)|_{fit} = 0.250(38)$ GeV^{-1} for the $P_1^7(Q^2)$ and $F_{\eta\gamma\gamma}(0)|_{fit} = 0.248(28)$ GeV^{-1} for the $P_2^2(Q^2)$, which translates into $\Gamma_{\eta\gamma\gamma}|_{fit} = 0.43(13)$ keV and $\Gamma_{\eta\gamma\gamma}|_{fit} = 0.42(10)$ keV, respectively. Comparing with the experimental value $\Gamma_{\eta\gamma\gamma}|_{exp} = 0.516(18)$ keV such predictions are at 0.66 and 0.94 standard deviation each.

3 Reanalysis of η-η' mixing parameters

In this section we briefly summarize the main elements to extract the mixing parameters exclusively from our fits to the form factor data. As was done in Ref. [3], we analyze η-η' mixing using the quark-flavor basis. In this basis, the η and η' decay constants are parametrized as

$$\begin{pmatrix} F_\eta^q & F_\eta^s \\ F_{\eta'}^q & F_{\eta'}^s \end{pmatrix} = \begin{pmatrix} F_q\cos\phi_q & -F_s\sin\phi_s \\ F_q\sin\phi_q & F_s\cos\phi_s \end{pmatrix} , \qquad (5)$$

where $F_{q,s}$ are the light-quark and strange pseudoscalar decay constants, respectively, and $\phi_{q,s}$ the related mixing angles. Several phenomenological analyses find $\phi_q \simeq \phi_s$, which is also supported by large-N_c ChPT calculations where the difference between these two angles is seen to be proportional to an OZI-rule violating parameter and hence small [43, 44].

Within this approximation, the asymptotic limits of the TFFs take the form

$$\begin{aligned} \lim_{Q^2\to\infty} Q^2 F_{\eta\gamma^*\gamma}(Q^2) &= 2(\hat{c}_q F_\eta^q + \hat{c}_s F_\eta^s) \\ &= 2(\hat{c}_q F_q\cos\phi - \hat{c}_s F_s \sin\phi) \ , \\ \lim_{Q^2\to\infty} Q^2 F_{\eta'\gamma^*\gamma}(Q^2) &= 2(\hat{c}_q F_{\eta'}^q + \hat{c}_s F_{\eta'}^s) \\ &= 2(\hat{c}_q F_q\sin\phi + \hat{c}_s F_s \cos\phi) \ , \end{aligned} \qquad (6)$$

and their normalization at zero

$$\begin{aligned} F_{\eta\gamma\gamma}(0) &= \frac{1}{4\pi^2}\left(\frac{\hat{c}_q F_{\eta'}^s - \hat{c}_s F_{\eta'}^q}{F_{\eta'}^s F_\eta^q - F_{\eta'}^q F_\eta^s}\right) \\ &= \frac{1}{4\pi^2}\left(\frac{\hat{c}_q}{F_q}\cos\phi - \frac{\hat{c}_s}{F_s}\sin\phi\right) \ , \\ F_{\eta'\gamma\gamma}(0) &= \frac{1}{4\pi^2}\left(\frac{\hat{c}_q F_\eta^s - \hat{c}_s F_\eta^q}{F_\eta^q F_{\eta'}^s - F_\eta^s F_{\eta'}^q}\right) \\ &= \frac{1}{4\pi^2}\left(\frac{\hat{c}_q}{F_q}\sin\phi + \frac{\hat{c}_s}{F_s}\cos\phi\right) \ , \end{aligned} \qquad (7)$$

with $\hat{c}_q = 5/3$ and $\hat{c}_s = \sqrt{2}/3$.

Experimental information provides $|F_{\eta\gamma\gamma}(0)|_{\rm exp} = 0.274\ (5)$ GeV^{-1} and $|F_{\eta'\gamma\gamma}(0)|_{\rm exp} = 0.344(6)$ GeV^{-1} and for the asymptotic value of the η TFF we take the value shown in Eq. (3) with symmetrical errors, $\lim_{Q^2\to\infty} Q^2 F_{\eta\gamma^*\gamma}(Q^2) = 0.177(15)$ GeV. With these values, the mixing parameters are predicted to be

$$F_q/F_\pi = 1.07(1) \ , \quad F_s/F_\pi = 1.39(14) \ , \quad \phi = 39.3(1.2)^\circ \ , \qquad (8)$$

with $F_\pi = 92.21(14)$ MeV [34]. The uncertainties are dominated by the error from the asymptotic value prediction.

The mixing parameters obtained with our fits are precise enough to be competitive with the standard approaches with the advantage of using much less input information.

4 A prediction for the $VP\gamma$ couplings

In this section, we extend our analysis to the vector-pseudoscalar electromagnetic form factors. In particular, we are interested in the couplings of the radiative decays of lowest-lying vector mesons into η or η', i.e., $V \to (\eta,\eta')\gamma$, and of the radiative decays $\eta' \to V\gamma$, with $V = \rho,\omega,\phi$.

We follow closely the method presented in Refs. [44, 45], and make use of the equations in Appendix A in Ref. [44] to relate the form factors with the mixing angle and the decay constants in the flavor basis. To account for the $\phi-\omega$ mixing we use $\phi_V = 3.4^\circ$. The form factors, saturated with the lowest-lying resonance and then assuming vector meson dominance, can be expressed by

$$F_{VP\gamma}(0,0) = \frac{f_V}{m_V} g_{VP\gamma} \, , \qquad (9)$$

where $g_{VP\gamma}$ are the couplings we are interested in, and f_V are the leptonic decay constants of the vector mesons and are determined from the experimental decay rates via

$$\Gamma(V\to e^+e^-) = \frac{4\pi}{3}\alpha^2 \frac{f_V^2}{m_V} c_V^2 \, , \qquad (10)$$

with c_V an electric charge factor of the quarks that make up the vector, $c_V = (\frac{1}{\sqrt{2}}, \frac{\sin\theta_V}{\sqrt{6}}, \frac{\cos\theta_V}{\sqrt{6}})$ for $V = \rho,\omega,\phi$ respectively. Here $\theta_V = \phi_V + \arctan(1/\sqrt{2})$. Experimentally we find

$$\begin{aligned} f_{\rho^0} &= (221.2\pm 0.9)\text{MeV} \, , \\ f_\omega &= (179.9\pm 3.1)\text{MeV} \, , \\ f_\phi &= (239.0\pm 3.8)\text{MeV} \, . \end{aligned} \qquad (11)$$

using $\Gamma(\rho\to e^+e^-) = 7.04(6)$ keV, $\Gamma(\omega\to e^+e^-) = 0.60(2)$ keV, and $\Gamma(\phi\to e^+e^-) = 1.27(4)$ keV from [34].

The couplings in this flavor basis are:

$$g_{\rho\eta\gamma} = \frac{3m_\rho}{4\pi^2 f_{\rho^0}} \frac{\cos\phi}{\sqrt{2}F_q}\,, \qquad g_{\rho\eta'\gamma} = \frac{3m_\rho}{4\pi^2 f_{\rho^0}} \frac{\sin\phi}{\sqrt{2}F_q}\,,$$
$$g_{\omega\eta\gamma} = \frac{m_\omega}{4\pi^2 f_\omega}\left(\cos\phi_V \frac{\cos\phi}{\sqrt{2}F_q} - 2\sin\phi_V \frac{\sin\phi}{\sqrt{2}F_s}\right),$$
$$g_{\omega\eta'\gamma} = \frac{m_\omega}{4\pi^2 f_\omega}\left(\cos\phi_V \frac{\sin\phi}{\sqrt{2}F_q} + 2\sin\phi_V \frac{\cos\phi}{\sqrt{2}F_s}\right),$$
$$g_{\phi\eta\gamma} = -\frac{m_\phi}{4\pi^2 f_\phi}\left(\sin\phi_V \frac{\cos\phi}{\sqrt{2}F_q} + 2\cos\phi_V \frac{\sin\phi}{\sqrt{2}F_s}\right),$$
$$g_{\phi\eta'\gamma} = -\frac{m_\phi}{4\pi^2 f_\phi}\left(\sin\phi_V \frac{\sin\phi}{\sqrt{2}F_q} - 2\cos\phi_V \frac{\cos\phi}{\sqrt{2}F_s}\right). \tag{12}$$

where we have assumed $\phi_q = \phi_s = \phi$. Table 1 collects our predictions in its second column. Corrections due to $\phi_q \neq \phi_s$ to these formulae can be found in Appendix A, Eq. (A.5) of Ref. [44].

The decay widths of $P \to V\gamma$ and $V \to P\gamma$ are

$$\Gamma(P \to V\gamma) = \frac{\alpha}{8} g^2_{VP\gamma}\left(\frac{m_P^2 - m_V^2}{m_P}\right)^3,$$
$$\Gamma(V \to P\gamma) = \frac{\alpha}{24} g^2_{VP\gamma}\left(\frac{m_V^2 - m_P^2}{m_V}\right)^3. \tag{13}$$

The experimental decay widths from [34] allow us to extract an experimental value for $g_{VP\gamma}$, which are collected in the last column on Table 1.

Our predictions compare well with the experimental determinations, see Table 1, specially considering the simplicity of the approach. The differences are always below 2 standard deviations, excepting the ω couplings. Our prediction for the ratio of J/Ψ decays is in that respect remarkable.

Table 1. Summary of VPγ couplings. Experimental determinations are from Ref. [34].

	Prediction	Experiment
$g_{\rho\eta\gamma}$	1.50(4)	1.58(5)
$g_{\rho\eta'\gamma}$	1.18(5)	1.32(3)
$g_{\omega\eta\gamma}$	0.57(2)	0.45(2)
$g_{\omega\eta'\gamma}$	0.55(2)	0.43(2)
$g_{\phi\eta\gamma}$	−0.83(11)	−0.69(1)
$g_{\phi\eta'\gamma}$	0.98(14)	0.72(1)
$R_{J/\Psi} = \frac{\Gamma(J/\Psi\to\eta'\gamma)}{\Gamma(J/\Psi\to\eta\gamma)}$	4.74(55)	4.67(20)

5 Conclusions

In the present work, the η transition form factor has been analyzed for the first time in both space- and time-like regions at low and intermediate energies making use of a model-independent approach based on the use of rational approximants of Padé type. The model independence of our approach is achieved trough a detailed and conservative evaluation of the systematic error associated to it. The new set of experimental data on the $\eta \to e^+e^-\gamma$ reaction provided by the A2 Collaboration in the very low-energy part of the time-like region allows for a much better determination of the slope and curvature parameters of the form factor, as compared to the predictions obtained in our previous work only using space-like data, which constitute the most precise values up-to-date of these low-energy parameters. Our method is also able to predict for the first time the third derivative of the form factor. In addition, the new analysis has served to further constrain its values at zero momentum transfer and infinity. We have seen that our results, in particular for the case of the slope parameter, are quite insensitive to the values used in the fits for the two-photon decay width of the η, thus showing that the collection of space- and time-like experimental data is more than enough to fix a value for the normalization of the form factor compatible with current measurements. We have also seen that the role played by the high-energy space-like data is crucial to get accurate predictions for the low-energy parameters of the form factor and its asymptotic value. As a consequence of these new results, we have fully reanalyzed the η-η' mixing parameters this time also considering renormalisation-scale dependent effects of the singlet decay constant F_0. The new values obtained are already competitive with standard results having the advantage of requiring much less input information. Related to this, we have also obtained predictions for the $VP\gamma$ couplings which are in the ballpark of present-day determinations.

In summary, the method of Padé approximants has been shown to be very powerful for fixing the low-energy properties of the η transition form factor making their predictions more accurate and well-established. This fact opens the door to a more exhaustive analysis of the single Dalitz decay processes $P \to l^+l^-\gamma$, with $P = \pi^0, \eta, \eta'$ and $l = e, \mu$, the double Dalitz ones $P \to l^+l^-l^+l^-$ (in all possible kinematically allowed configurations) [46], and the rare lepton-pair decays $P \to l^+l^-$ —see the $\pi^0 \to e^+e^-$ application in Ref. [47], which are usually discussed only in terms of monopole approximations. Indeed, when this work was being concluded the BESIII Collaboration reported a first observation of the $\eta' \to e^+e^-\gamma$ process measuring the branching ratio and extracting the η' transition form factor [48]. This new measurement may put our approach with its back to the wall. However, a very preliminary analysis of this recent data in comparison with our prediction for this form factor in the time-like region exhibits a nice agreement but reveals the necessity of going beyond the vector meson dominance model used in the experimental analysis [49].

This work was supported in part by the the Ministerio de Ciencia e Innovación under grant FPA2011-25948, the Ministerio de Economía y Competitividad under grants CICYT-FEDER-FPA 2014-55613-P and SEV-2012-0234, the Secretaria d'Universitats i Recerca del Departament d'Economia i Coneixement de la Generalitat de Catalunya under grant 2014 SGR 1450, and the Spanish Consolider-Ingenio 2010 Programme CPAN (CSD2007-00042).

References

1 L. Ametller, J. Bijnens, A. Bramon and F. Cornet, Phys. Rev. D **45** (1992) 986.
2 H. Czyz, S. Ivashyn, A. Korchin and O. Shekhovtsova, Phys. Rev. D **85** (2012) 094010 [arXiv:1202.1171 [hep-ph]].
3 R. Escribano, P. Masjuan and P. Sanchez-Puertas, Phys. Rev. D **89** (2014) 3, 034014 [arXiv:1307.2061 [hep-ph]].
4 C. Hanhart, A. Kupsc, U.-G. Meissner, F. Stollenwerk and A. Wirzba, Eur. Phys. J. C **73** (2013) 2668 [arXiv:1307.5654 [hep-ph]].
5 Y. Klopot, A. Oganesian and O. Teryaev, JETP Lett. **99** (2014) 679 [arXiv:1312.1226 [hep-ph]].
6 R. I. Dzhelyadin *et al.* [Lepton-G Collaboration], Phys. Lett. B **94** (1980) 548 [Sov. J. Nucl. Phys. **32** (1980) 516] [Yad. Fiz. **32** (1980) 998].
7 H. J. Behrend *et al.* [CELLO Collaboration], Z. Phys. C **49** (1991) 401.
8 J. Gronberg *et al.* [CLEO Collaboration], Phys. Rev. D **57** (1998) 33 [hep-ex/9707031].
9 R. Arnaldi *et al.* [NA60 Collaboration], Phys. Lett. B **677** (2009) 260 [arXiv:0902.2547 [hep-ph]].
10 H. Berghauser *et al.* [A2 Collaboration], Phys. Lett. B **701** (2011) 562.
11 M. Hodana *et al.* [WASA-at-COSY Collaboration], EPJ Web Conf. **37** (2012) 09017 [arXiv:1210.3156 [nucl-ex]].
12 P. Aguar-Bartolome *et al.* [A2 Collaboration], Phys. Rev. C **89** (2014) 4, 044608 [arXiv:1309.5648 [hep-ex]].
13 P. Kroll, Eur. Phys. J. C **71** (2011) 1623 [arXiv:1012.3542 [hep-ph]].
14 A. E. Dorokhov, A. E. Radzhabov and A. S. Zhevlakov, Eur. Phys. J. C **71** (2011) 1702 [arXiv:1103.2042 [hep-ph]].
15 S. J. Brodsky, F. G. Cao and G. F. de Teramond, Phys. Rev. D **84** (2011) 033001 [arXiv:1104.3364 [hep-ph]].
16 S. J. Brodsky, F. G. Cao and G. F. de Teramond, Phys. Rev. D **84** (2011) 075012 [arXiv:1105.3999 [hep-ph]].
17 Y. N. Klopot, A. G. Oganesian and O. V. Teryaev, Phys. Rev. D **84** (2011) 051901 [arXiv:1106.3855 [hep-ph]].
18 X. G. Wu and T. Huang, Phys. Rev. D **84** (2011) 074011 [arXiv:1106.4365 [hep-ph]].
19 S. Noguera and S. Scopetta, Phys. Rev. D **85** (2012) 054004 [arXiv:1110.6402 [hep-ph]].
20 I. Balakireva, W. Lucha and D. Melikhov, Phys. Rev. D **85** (2012) 036006 [arXiv:1110.6904 [hep-ph]].
21 D. Melikhov and B. Stech, Phys. Rev. D **85** (2012) 051901 [arXiv:1202.4471 [hep-ph]].
22 P. Kroll and K. Passek-Kumericki, J. Phys. G **40** (2013) 075005 [arXiv:1206.4870 [hep-ph]].
23 D. Melikhov and B. Stech, Phys. Lett. B **718** (2012) 488 [arXiv:1206.5764 [hep-ph]].
24 C. Q. Geng and C. C. Lih, Phys. Rev. C **86** (2012) 038201 [Erratum-ibid. C **87** (2013) 3, 039901] [arXiv:1209.0174 [hep-ph]].
25 Y. Klopot, A. Oganesian and O. Teryaev, Phys. Rev. D **87** (2013) 036013 [arXiv:1211.0874 [hep-ph]].
26 J. Bijnens, A. Bramon and F. Cornet, Phys. Rev. Lett. **61** (1988) 1453.
27 J. Bijnens, A. Bramon and F. Cornet, Z. Phys. C **46** (1990) 599.
28 P. Masjuan, Phys. Rev. D **86** (2012) 094021 [arXiv:1206.2549 [hep-ph]].
29 G. A. Baker and P. Graves-Morris, *Padé Approximants*, Encyclopedia of Mathematics and its Applications, Cambridge University Press (1996).
30 P. Masjuan, S. Peris and J. J. Sanz-Cillero, Phys. Rev. D **78** (2008) 074028 [arXiv:0807.4893 [hep-ph]].
31 P. Masjuan Queralt, arXiv:1005.5683 [hep-ph].
32 G. P. Lepage and S. J. Brodsky, Phys. Rev. D **22** (1980) 2157.
33 P. del Amo Sanchez *et al.* [BABAR Collaboration], Phys. Rev. D **84** (2011) 052001 [arXiv:1101.1142 [hep-ex]].
34 K. A. Olive *et al.* [Particle Data Group Collaboration], Chin. Phys. C **38** (2014) 090001.
35 D. Babusci *et al.* [KLOE-2 Collaboration], JHEP **1301** (2013) 119 [arXiv:1211.1845 [hep-ex]].
36 B. Aubert *et al.* [BABAR Collaboration], Phys. Rev. D **74** (2006) 012002 [hep-ex/0605018].
37 S. J. Brodsky and G. P. Lepage, Phys. Rev. D **24** (1981) 1808.
38 B. Kubis and J. Plenter, Private communication, arXiv:1504.02588 [hep-ph].
39 P. Masjuan and S. Peris, JHEP **0705** (2007) 040 [arXiv:0704.1247 [hep-ph]].
40 P. Masjuan and S. Peris, Phys. Lett. B **663** (2008) 61 [arXiv:0801.3558 [hep-ph]].
41 P. Masjuan, E. Ruiz Arriola and W. Broniowski, Phys. Rev. D **87** (2013) 1, 014005 [arXiv:1210.0760 [hep-ph]].
42 P. Masjuan and M. Vanderhaeghen, arXiv:1212.0357 [hep-ph].
43 T. Feldmann, P. Kroll and B. Stech, Phys. Rev. D **58** (1998) 114006 [hep-ph/9802409].
44 R. Escribano and J. M. Frere, JHEP **0506** (2005) 029 [hep-ph/0501072].
45 P. Ball, J. M. Frere and M. Tytgat, Phys. Lett. B **365** (1996) 367 [hep-ph/9508359].
46 R. Escribano and S. González-Solís, arXiv:1511.04916 [hep-ph].
47 P. Masjuan and P. Sanchez-Puertas, arXiv:1504.07001 [hep-ph].
48 M. Ablikim *et al.* [BESIII Collaboration], Phys. Rev. D **92** (2015) 1, 012001 [arXiv:1504.06016 [hep-ex]].
49 R. Escribano, S. González-Solís, P. Masjuan and P. Sanchez-Puertas, work in preparation.